Lattice modeling and testing of aerated autoclaved concrete infilled frames

Aydin, Beyazit B.; Binici, Baris ; Hendriks, Max A.N.; Tuncay, Kagan

DOI
10.1016/j.engstruct.2021.113467

Publication date
2022

Document Version
Final published version

Published in
Engineering Structures

Engineering Structures 251 (2022) 113467

Contents lists available at ScienceDirect

Engineering Structures

journal homepage: www.elsevier.com/locate/engstruct

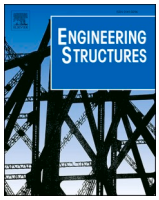

Lattice modeling and testing of aerated autoclaved concrete infilled frames

Beyazit B. Aydin [a,*], Baris Binici [a], Max A.N. Hendriks [b,c], Kagan Tuncay [a]

[a] Department of Civil Engineering, Middle East Technical University (METU), Ankara, Turkey
[b] Faculty of Civil Engineering and Geosciences, Delft University of Technology (TU Delft), Delft, the Netherlands
[c] Department of Structural Engineering, Norwegian University of Science and Technology (NTNU), Trondheim, Norway

ARTICLE INFO

Keywords:
Modeling
Cracks & cracking
Infilled walls

ABSTRACT

Significant infill wall damage in reinforced concrete frame buildings was observed in the past earthquakes. A vast number of numerical approaches have been proposed to estimate the non-linear behavior of infilled frames at different scales. Mesoscale lattice models were successfully used in the past to simulate the behavior of reinforced concrete member response. In this study, two-dimensional mesoscale lattice approach with an extended calibration technique was consistently applied to simulate the response of unreinforced Aerated Autoclaved Concrete (AAC) masonry infilled reinforced concrete frames. Two AAC infilled walls were tested for the purposes of this study. The objective of the tests were to investigate the effect of infilled wall-frame interaction with and without openings and validate the proposed numerical approach. In addition to the tests conducted, two tests were used from the literature for further validation. The maximum error of load capacity estimation from the simulations was less than 15% for all the examined tests. The proposed lattice model was capable of estimating crack propagation in the infill walls with reasonable accuracy. The frame-infill wall interaction was successfully simulated with providing a realistic representation of strut formation. Finally, a parametric study was conducted to examine contact length and strut width as a function of lateral deformation. The results show that the infill wall-frame contact length is significantly dependent on the lateral deformation demand levels and properties of interaction region.

1. Introduction

Infill walls made of aerated autoclaved concrete (AAC), blocks, etc. are used worldwide to separate and isolate regions. They are considered as non-structural elements in structural design, however, they improve the rigidity and lateral strength of the structural system. Past earthquakes (Van, Kocaeli, Bingol, Messina, Carlentini, L'Aquila, Wenchuan, Abruzzo, Northridge, Emilia Earthquakes) have shown that infill walls may sustain considerable damage under moderate to severe ground motions. Nevertheless, the collapse of infill walls may create asymmetry in structures, might trigger heavy-damage and may cause loss of life. Significant loss has been noted due to the infill wall damage [1–5]. Hence, the performance limit states of infill walls should be controlled accurately.

Infill walls are generally not included in the analysis and design of frame buildings except their mass and weight. This practical approach would be correct if no interaction occurred between the infill walls and the frame. The observed damage in the infill walls after earthquakes indicate that energy absorption and contribution of the infill walls to the lateral load carrying capacity can be significant. Understanding the frame-infill interaction has been the subject of numerous studies since the 1950's [6] including experimental studies [7–10] and analytical investigations [11–14]. However, interaction could not be fully understood due to the lack of detailed simulations, and presence of several parameters such as the mechanical properties of mortar, the wall geometry, and space between frame and infill effecting the response [15]. Hence, explaining the force flow over the infill walls is necessary in order to define the effect of walls on global response.

Among many numerical approaches to model infill walls, there are three mainstream directions: macroscale, mesoscale and microscale models. While the elements used in the microscale simulations are in the few millimeters order, macroscale models are employed with larger element size. The most performed macroscale model is placing one or more struts for the walls [16–22]. The contact regions between frames and infill walls are assumed constant at the corners in most of the models. The key disadvantage of these models is the difficulty of

* Corresponding author.
E-mail addresses: beyazit@metu.edu.tr (B.B. Aydin), binici@metu.edu.tr (B. Binici), m.a.n.hendriks@tudelft.nl (M.A.N. Hendriks), tuncay@metu.edu.tr (K. Tuncay).

https://doi.org/10.1016/j.engstruct.2021.113467
Received 8 May 2021; Received in revised form 26 September 2021; Accepted 21 October 2021
Available online 12 November 2021

estimating strut properties. The existing strut models in American [23] and Canadian [24] codes cannot accurately predict the rigidity, strength, and ductility properties of infill walls, as shown by Turgay et al. [25]. Furthermore, strut behavior becomes more unpredictable when openings exist in the wall. The strut based macro models do not provide information on the local behavior, interface opening and cracking. In order to overcome these deficiencies, finite element models (FEM) were employed by many researchers for micro and mesoscale approaches [26–31]. Both continuum and discrete finite element approaches were developed in those studies. Two different finite element approaches were employed, in which the wall units (brick, autoclaved aerated concrete (AAC) and mortar) were either modelled separately (microscale) or homogenized (mesoscale) [32–38]. The use of micro and mesoscale elements may provide a more realistic response estimation for crack propagation and damage patterns. However, they have classical drawbacks of finite element models, such as the pre- and post- processing difficulties due to defining interface elements between individual bricks, computational inefficiencies and limited applications in practice [39]. Calibration of the mesoscale constitutive models involving a combination of different elements and description of the interaction region are the other challenges for these class of models [40].

Particle-based and lattice simulations were proposed in the last few decades to estimate the fracturing and damage for concrete and reinforced concrete (RC) members in order to overcome the aforementioned disadvantages of FEM. Aydin et al. [41–43] proposed a lattice model with a non-linear tension and elastic compression behavior, which was successfully validated for the nonlinear response of concrete and RC members and did not conduct any work on masonry. In their approach, concrete compressive behavior is simulated as indirect tension failure. The model was validated with experimental results from tests on concrete and reinforced concrete members extensively. Many different types of elements have been used by many researchers for modeling, such as shear springs [44–49], Bernoulli-Euler beams [50–53], etc. One advantage of introducing rotational degrees of freedom is improving limitation on Poisson's ratio, which varies between 0.26 and 0.42 depending on the rotation of loading axis in truss lattice networks. However, due its conceptual simplicity, the use of few input parameters and success in modeling fracture, lattice modeling composed of truss networks is still commonly preferred for nonlinear simulations [54–57]. This direction has been the choice in this work. The model proposed by Aydin et al. [41–43] differs from the other lattice approaches in the following aspects: i-calibration of material constitutive models to match the average response within characteristic length, ii- assumption of homogeneous material properties for discrete lattice elements while calibrating multilinear softening curve in tension and applying randomness through mesh perturbation controlled with randomization in compression for the treatment of inhomogeneity so as to preserve practicality, and iii- modeling compression failure as an indirect tension failure rather than plasticity based constitutive model for concrete in compression.

Lattice Discrete Particle Model developed by Cusatis and co-workers [58–59] was utilized to simulate mortar [60–61], masonry and masonry interaction with mortar [62–64] with a good accuracy in order to simulate multi-materials and multi-material domains (i.e. masonry and RC) as a particle based model. On the other hand, the application of lattice models for multi-material domains is very limited [65]. Modeling anisotropic behavior of masonry units and multi-material media with a lattice network are the key difficulties in these models. Thus, none of these models was utilized for the application of AAC infill walls in the literature. It is hypothesized that the practical and easy-to-implement model of Aydin et al. [41–43] has a great potential to model AAC infilled wall structures as well.

In this study, a mesoscale two dimensional lattice model for the four AAC masonry infilled reinforced concrete (RC) frames was developed for the first time in the literature to the best of authors' knowledge. A consistent modelling approach was developed that differs from the previous lattice models [41–43] as it employs bi-material idealization in the lattice models, for AAC and concrete, with a special emphasis on the interface between these materials. Two single-bay and single-story half-scaled AAC infilled portal frames were tested to investigate the effect of interaction behavior and wall openings on the global response by comparing the lattice simulation results and to validate the proposed approach along with the two additional AAC infilled frames taken from literature [66–67]. The key objectives of the study are: 1- to propose a lattice modelling approach with model calibration steps for AAC walls, 2- to investigate the effect of interaction behavior and wall openings on the global response by conducting two AAC infilled frames tests, 3- to validate the proposed approach with four AAC infilled wall experiments, 4- to study the contact length behavior for different aspect ratios of infilled frames as a function of lateral deformation. All the test cases presented in the study have an axis of symmetry along the loading direction and were subjected to in-plane loading only. Thus, two-dimensional modeling is conducted instead of using three-dimensional models for the sake of computational efficiency. Meso-scale models can indeed be two-dimensional and they are capable of simulating AAC masonry and masonry infilled wall behavior as presented past studies [30,68–69].

While the inter-story drift limits are given in the codes to examine performance limit states of infill walls, the damage limit states are not detailed for both fragile and deformable components. The research outcome from this work can help in estimating damage limit state of infill walls at different deformation levels. For this purpose, a sub-structure lattice model composed of one bay one-story infilled RC frame can be constructed and inter-story deformations can be imposed on this model to estimate the damage limit state of the infill walls.

2. Lattice model

Aydin et al. [41–42] proposed a lattice model based on a two-dimensional truss network with uniformly distributed nodes. Only translational motion is utilized for each element while shear transmission and rotation in a region is available for a lattice unit rather than element-wise. The modulus of elasticity (E) multiplied by the cross-sectional area (A) of the truss elements is taken as the same for all elements and obtained from a simple energy principle [41]. The model comprises three types of elements: concrete, steel, and bond elements. The element types and corresponding constitutive models are shown in Fig. 1. Force-strain curves are adopted for the nonlinear response of the elements due to use using EA value. For this reason, ultimate and yield forces (F_{ult} and F_{yield} , respectively) at the yield and ultimate strains (ε_{ult} and ε_{yield} , respectively) for steel elements, critical force (F_{cr}) at critical strain (ε_{cr}) for concrete elements are used. The softening parameters, a_1 , a_2 , a_3 of the tensile behavior of concrete and AAC truss elements (Fig. 1) are found such that lattice simulation result of tensile stress deflection curve matches the uniaxial stress-average displacement response of the tension test result. In the absence of reliable test data, the stress-displacement model of Cornelissen et al. [70] was employed as the "correct" test result for the softening part and the calibration of the input parameters were conducted based on those results. Further detail can be found in Aydin et al. [41–42]. Isotropic behavior on fracture energy was obtained by utilizing constitutive models of elements based on their lengths. Thus, the crack propagation in any direction can be obtained objectively. Tension calibration is detailed in the workflow figure (Fig. 2). Hence, the softening response within the gauge length is exhibited although brittle softening is assigned to concrete elements. In the light of information on mesh sensitivity in previous works conducted for concrete and RC members [41–43], it can be stated that fracture energy regularization enables mesh independence in *meso*-scale. Thus, different grid size could be utilized with mesh objectivity. The unloading rules of the elements are origin-oriented for the tension model. Bond elements connecting concrete and steel nodes exhibit elastic brittle

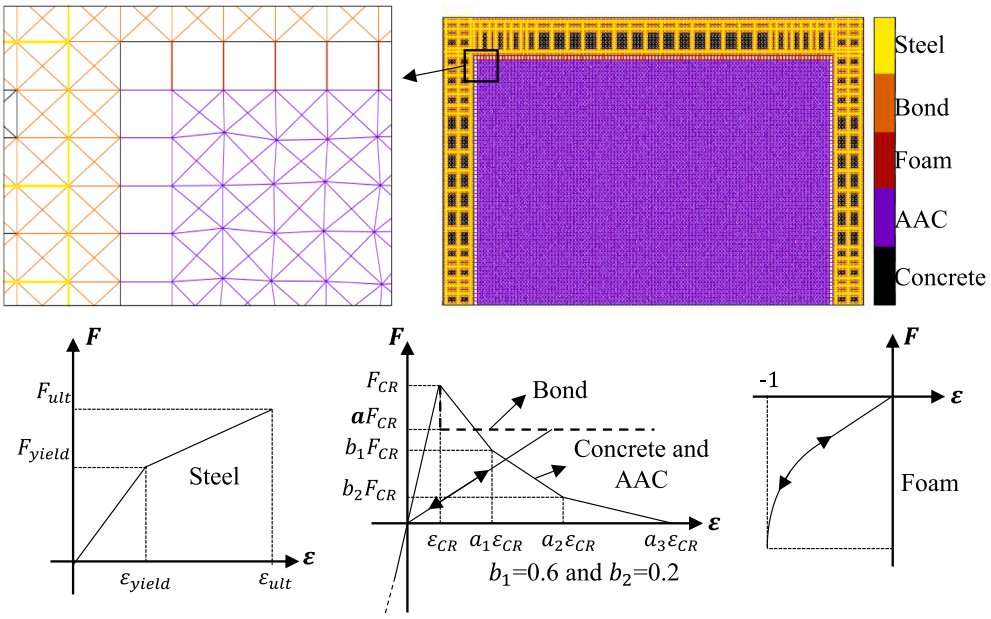

Fig. 1. Overview of the modeling approach: randomized mesh, element types and corresponding constitutive models for Concrete, AAC, Bond, Foam and Steel Elements.

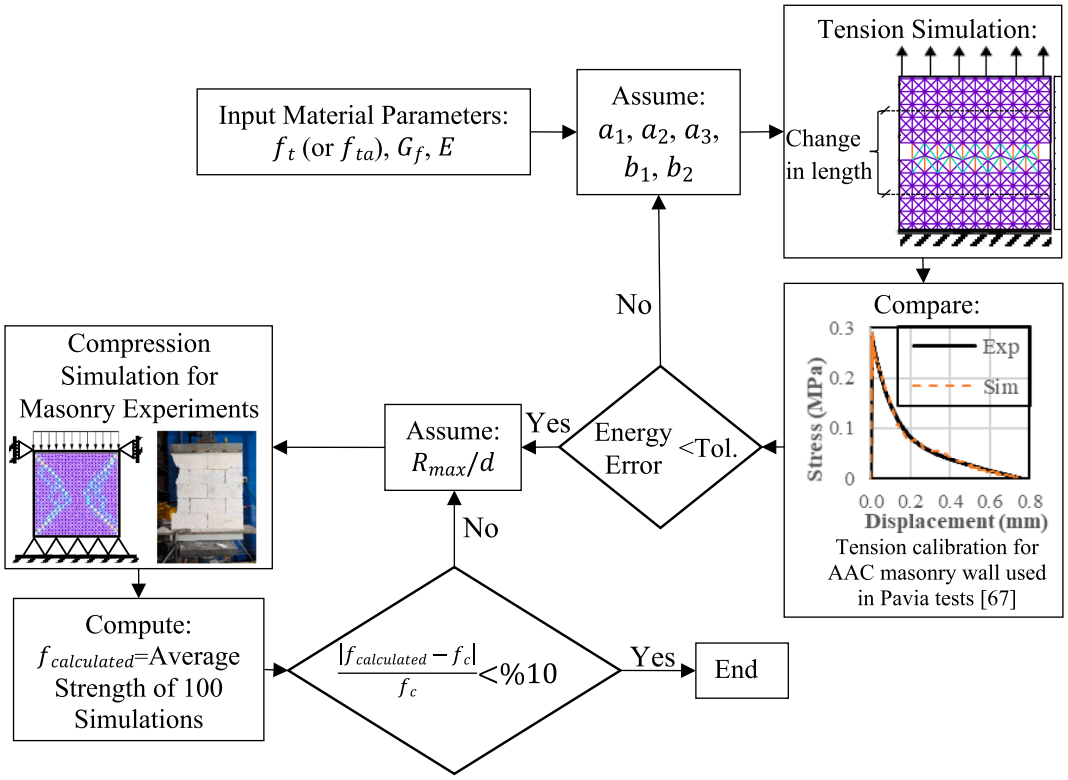

Fig. 2. Workflow for tension and compression calibration by adjusting the maximum grid.

response with residual strength to ensure that the slip behavior is reflected accurately based on RC simulation results conducted by Aydin et al. [41–43]. The residual bond strength parameter (α) was chosen with the following formulation by equating ultimate bond force to bond elements in lattice network;

$$\alpha = \frac{\tau_b \pi d_b}{0.621 w f_t \sqrt{2}} \quad (1)$$

Where τ_b is the residual bond strength, d_b is longitudinal bar diameter, f_t is tensile strength of concrete, w is the member thickness.

Compressive stress–strain response of the concrete elements is assumed linear and compression failure is accounted as a consequence of tension failure with the novelty of grid perturbation, as visible at the top left of Fig. 1 [43]. The unstructured grid topology was formed by perturbing a structured grid with grid size (d); the grid perturbance magnitude (R/d) varied between zero and the maximum grid

perturbance magnitude (R_{max}/d) at a random angle of θ between zero and 360 degrees, both with uniform probability distributions for compression calibration of the model. The calibration of the R_{max}/d value and the tensile softening parameters were slightly modified to include the bi-material presence (Fig. 2). The R_{max}/d value was calibrated by comparing the average compression strength of 100 compression simulations, with 100 different grid perturbation instances, with the mean value of the compressive strength from uniaxial compression AAC masonry tests with an acceptable error of 10% based on engineering judgement and computational efficiency. Based on preliminary simulations, it was found that 100 cases should be simulated in order to obtain accurate results for material strength estimations. Homogeneous material properties were assumed by calibrating multilinear softening curve in tension to represent the behavior within characteristic length and applying randomness through mesh perturbation controlled with R_{max}/d in compression for the treatment of inhomogeneity so as to preserve practicality. Orthogonal elements to force flow direction in a lattice unit provide the internal friction with the tensile fracture energy and mesh perturbation, which allows triggering of the instability initiated by internal cracking.

Explicit integration solution scheme with proportional integral derivative (PID) algorithm was conducted to solve nonlinear behavior of the model under monotonic loading. Further explanation on the application of the PID scheme in explicit dynamic simulations can be found in Aydin et al. [42–43]. All simulations in this study were performed with sufficiently low loading velocities to simulate quasi-static loading conditions and to eliminate dynamic amplification effects similar to a nonlinear static push-over test. The lumped mass was defined for each node. The proposed model was validated by simulating numerous experimental works that have different failure type including flexural, shear, tensile, compressive failures and combination of them accurately [41–43] by utilizing proposed tension and compression calibration procedures. It was found that tension only modeling along with the grid disturbance parameters allow different failure modes. Proposed lattice approach is also capable of modeling uniaxial compression tests with different boundary conditions affecting significantly the strength and softening regime of concrete [43].

Two additional element types, in addition to the original reinforced concrete model, are defined. The first one represents the AAC masonry elements, which also adopts the concept of a piecewise linear softening diagram for the tensile regime. Secondly, a special interface element, called “foam element”, was introduced to simulate the interaction regions filled with foam between the wall and reinforced concrete frame members. The behavior of the interface elements connecting the AAC wall and concrete elements with foam material is selected as hyperelastic in compression, while the capacity is assumed as zero in tension (bottom right in Fig. 1). The compressive modulus of elasticity multiplied by the cross-sectional area of foam elements is formulated as

$$EA(\varepsilon) = (EA)_i + (EA)_i(m_t - 1)(-\varepsilon)^{n-1} \quad \text{for} \quad \varepsilon \leq 0 \tag{2}$$

where ε is the strain, $(EA)_i$ is the initially defined modulus of elasticity multiplied by the cross-sectional area, n is the parameter adjusting the polynomial degree and m_t is the multiplication value of initial $(EA)_i$ at strain value of -1. The same formulation is applicable for the unloading branch so that no energy dissipation can occur. In the interface region the diagonal elements of the lattice framework were removed due to the very low shear resistance of the foam or leveling mortar. Deformed shape was utilized to establish proper modeling in large deformations in the elements. Geometric nonlinearity was incorporated for all the elements except the interface elements so that only interaction in the normal direction was considered.

3. AAC infilled frames experiments

In this section, experiments of two unreinforced AAC masonry infilled frames are explained. The test results are presented and discussed. Two additional infilled frames tested by Binici et al. [66] and Penna and Calvi [67] are introduced to compare the results with lattice simulations in Section 5.

3.1. New tests in this study

Two single-bay and single-story half-scaled AAC infilled portal frames were tested in the course of this experimental program. The presence of the opening in the infill wall and its effect on the compression strut was studied with these specimens. The details and dimensions of the specimens named as SP1 and SP2 are shown in Fig. 3a,b. The dimensions and reinforcement detailing of the test frame, used for SP1 and SP2, are shown in Fig. 4a. The mechanical properties of concrete and rebar are provided in Table 1. Concrete used in the tests of this study had water/cement ratio, cement type and maximum aggregate size as 0.65, CEM1 42,5R and 11.2, respectively with the target cylindrical compressive strength of 25 MPa. Three uniaxial compression tests of 150 mm × 300 mm cylinders [71] were tested at the test days to determine compressive strength of concrete. According to ASTM C617 [72], sulfur caps were placed at the both ends to achieve plane surface. The RC frames were designed following the Turkish Earthquake Design Code [73] requirements. While the SP1 specimen had no opening, a window opening was placed in the wall for the SP2 specimen. The upper gap between the beam and the infill wall was adjusted as 1 cm and filled with foam for both specimens. On the other hand, leveling mortar was placed at the left and right interaction regions. Concentrated axial forces with a magnitude of 180 kN (0.18 × compressive strength (f_c) × gross section of columns) were applied on the columns with hydraulic actuators to simulate the axial forces from upper stories. Also, a distributed load was performed by placing steel blocks representing the dead plus reduced live loads (10.25 kN/m) on the slabs. The lateral load was then applied with a displacement control feedback. Lateral displacement reached positive and negative target drift ratios twice and drifts were increased by 0.5% at each cycle. The same loading procedure was applied for both infill wall specimens, SP1 and SP2.

Digital image correlation (DIC) was conducted to observe the local strain concentrations during tests. For this purpose, small black points were created randomly on a single face of the specimens. The average diameter of the black dots is around 0.6 mm. The spacing of these points ranges from 1.5 mm to 3.5 mm for uniaxial compression tests of masonry and infill wall. The photographs were taken with a 24 megapixel camera. Although out-of-plane motion of the specimens can introduce error in two dimensional DIC according to Mojsilovic and Salmanpour [74], accurate results of using only single camera for in-plane infill experiments were proposed by many researchers [75–78]. It was ensured that the rods was placed at the top of the infill wall specimens in order to prevent out-of-plane deformation. It should be noted that the main aim was to visualize cracking patterns with DIC since a relatively large area was photographed. Thus, crack width and strain measurements were beyond the limitation of the camera resolution.

Three AAC masonry wallettes with a thickness (w) of 10 cm were prepared according to TS EN 1052–1 [79] to perform uniaxial compression test. The dimensions and installed instrumentations are shown in Fig. 5a. Ball joints providing to rotate the end plates at the top of the upper side were used to avoid undesired moments. AAC units used in this study were the same as the units used in Todorovic et al. [80] (Fig. 5b). Test setup and DIC results are shown in Fig. 5c. Color contours represent the displacement of the points in lateral direction and major strain distribution obtained from DIC, overlapping with the crack patterns on the same image. The compressive strength results of three tests were determined as 1.20 MPa, 0.90 MPa and 0.87 MPa. Todorovic et al. [80] found that the mean compressive strength of five masonry prisms with dimensions (width × thickness) of 300 × 100 mm was 0.97 MPa, while the average value obtained from our tests was 0.99 MPa. Compressive stress and average displacement measured from left and

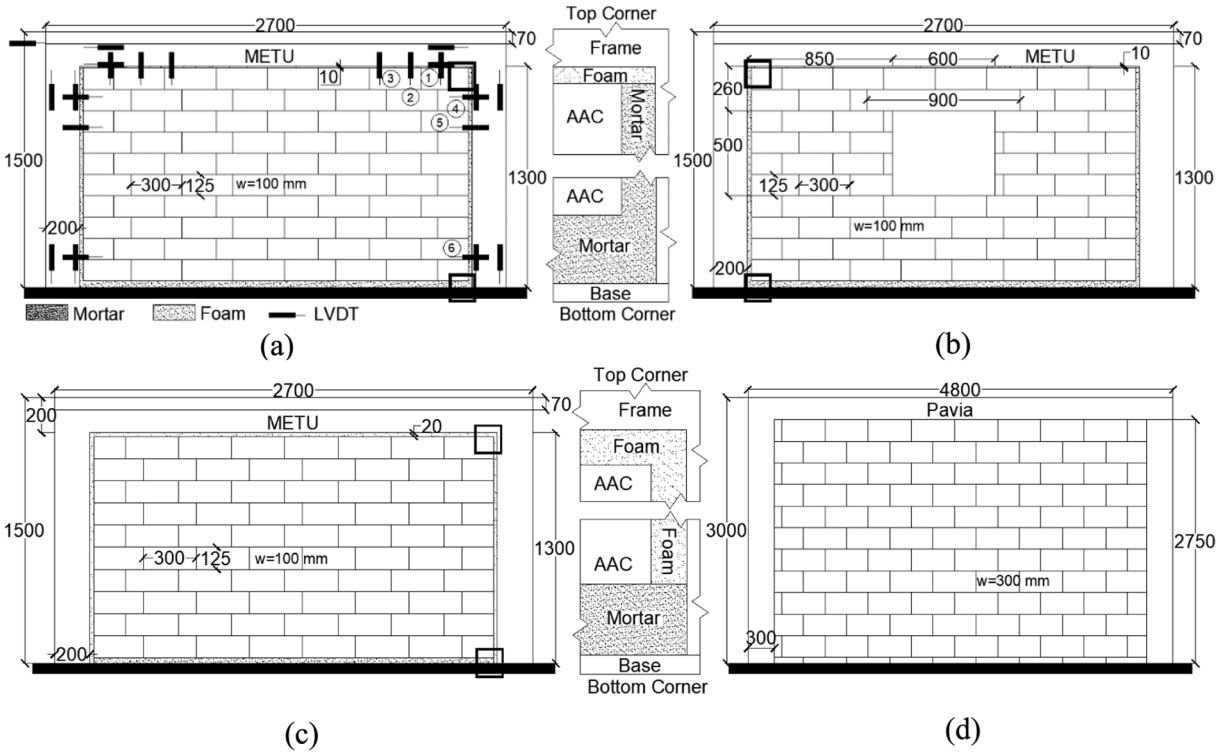

Fig. 3. Dimensions and installed instrumentations and zoomed corner of interface regions of the AAC infilled frames used for Batch 1 frames and AAC blocks as (a) SP1, (b) SP2 and (c) Binici et al. [66] and Batch 2 as (d) Penna and Calvi [67] (dimensions in mm).

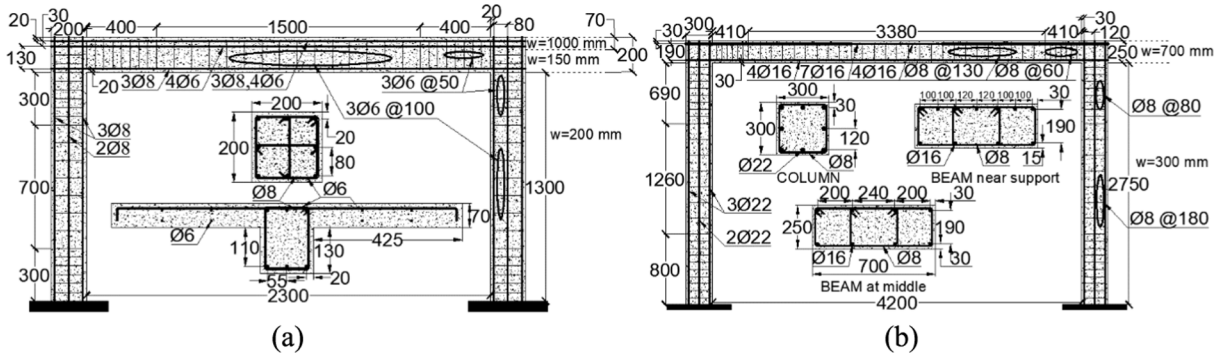

Fig. 4. The dimensions of frames used in infill wall experiments for (a) METU (Batch 1) Frame [66] and (b) Pavia (Batch 2) Frame [81] (dimensions in mm).

right Liner Variable Differential Transformers (LVDT), and the crack pattern at the end of the experiment for specimen 2 are shown in Fig. 5d, e. Brittle response with sudden drop after peak load and higher capacity than the other two specimens was exhibited by Test 1. The softening portion of that specimen could not be obtained due to the malfunctioning of LVDT controlling the induced displacement. Furthermore, it should be noted that the compression calibration of the model is conducted according to mean strength of 8 tests, including tested in this study and Todorovic et al [80].

The lateral load and displacement responses, the local response measured with LVDTs, and crack patterns at various drift ratios, 1.0% and 3.0% for positive and 3.0% for negative directions, are shown in Fig. 6,7 for SP1 and SP2. The plastic hinging of members is illustrated in the same figures by using the measured curvature values from the LVDTs located at the end sections.

The lateral load carrying capacity of SP1 was found as 96.4 kN for positive and 105.4 kN for negative loading directions, respectively. The yield load carrying capacity was found at a lateral displacement value of about 16 mm, and no capacity drop was observed until the 3.0% drift ratio, at which the experiment was finished for SP1. On the other hand, for SP2 a maximum load which was about 25% less than that observe in SP1 occurred at a displacement of about 50 mm until the end of the experiment (at a 4.0% drift ratio). Thus, strength degradation was not found for either of the specimens.

The maximum crack width at the wall was measured as 0.75 mm and 1.5 mm at the 0.35% drift ratio at which the first cracking was experienced for SP1 and SP2. First cracks on the columns were observed for a drift ratio of 0.5%. The main crack was a diagonal crack with a shear sliding mode at the mid-region for SP1. With increasing deformation demands, additional cracks were observed as shown in Fig. 6. For specimen SP2, inclined cracks were observed on both sides of the opening, indicating the lack of formation of the diagonal compression strut (Fig. 7).

3.2. Tests from literature

Two additional unreinforced AAC masonry infilled frames tested by Binici et al. [66] and Penna and Calvi [67] (Fig. 3c,d) are used to

Table 1
Material properties of concrete and steel.

Properties	Batch 1 (METU)	Batch 2 (Pavia)[a]	
Concrete		Column	Beam
Compression Strength (f_c) [MPa]	27.94[b] 25.00[c]	29.32	34.56
Tension Strength (f_t) [MPa]	1.85[d]	2.31	2.67
Density [kg/m^3]	2400	2500	
Modulus of Elasticity (E) [GPa]	24.5[e]	24.3	25.5
Fracture Energy (G_f) [N/m]	70[f]	94	97
a_1 [g]	1.5		
a_2	80.5	50.0	40.0
a_3	350.0	300.0	270.0
Long. Reinforcement			
Modulus of Elasticity [GPa]	200		
Yield Strength [MPa]	448[b] 456[c]	558	
Ultimate Strength [MPa]	535	649	
Ultimate Strain (ε_{ult})	0.1	0.023	
τ_b [MPa][h]	3.9	4.2	

[a] Values were taken from Milanesi et al.[30]
[b] Binici et al.[66]
[c] In this study
[d] TS500 [88]
[e] ACI 318 [89]
[f] CEB FIP Model Code 2010 [90]
[g] Fracture energy parameters were found for grid size (d) = 5 mm
[h] Calculated as $0.78\sqrt{f_c}$

compare the global responses for different types of interactions and to validate the models with four specimens in total in the next section. The dimensions of the test frame used in our experiments are the same as those used by Binici et al. [66], labeled as METU specimens (Fig. 4a). The same loading protocol was employed, i.e. axial forces on the columns and distributed load on the slabs were performed with a magnitude of 180 kN and 10.25 kN/m, respectively. The only difference with respect to the specimens SP1 and SP2 was observed at the region between wall and frame. In Binici et al. [66] the foam was placed on all 3 sides instead of only on the upper side as in our experiments. Also, the gap between the beam and the infill wall, which was 2 cm in the study by Binici et al. [66], was twice the thickness of the gap in SP1 and SP2. On the contrary, the test specimen proposed by Penna and Calvi [67], using the same RC frame of the research by Calvi and Bolognini [81] (Fig. 4b), had no gap between concrete and wall. In their study, single-bay and single-story full-scaled AAC infilled wall was subjected to in-plane tests under constant axial load and increasing cyclic lateral displacement excursions. While the axial load applied on the columns was 400 kN, beam had no distributed load.

In summary, two experimental campaigns composed of two different types of AAC masonries and bare frames for the four AAC infilled wall specimens are used for the simulations in this study. The first batch was the experiments tested at the Middle East Technical University (METU) while the second batch was carried out at the University of Pavia (Pavia). Material properties of used AAC masonries are given in Table 2. It should be noted that "batch" term refers a set of one AAC wall and one RC frame in this study.

Envelope curves of three cyclic experiments, SP1, SP2, Binici et al. [66] and bare frame capacity results, are provided in Fig. 7 in order to discuss wall contributions for batch 1. Different types of frame-infill interaction properties affect the contributions as expected. For

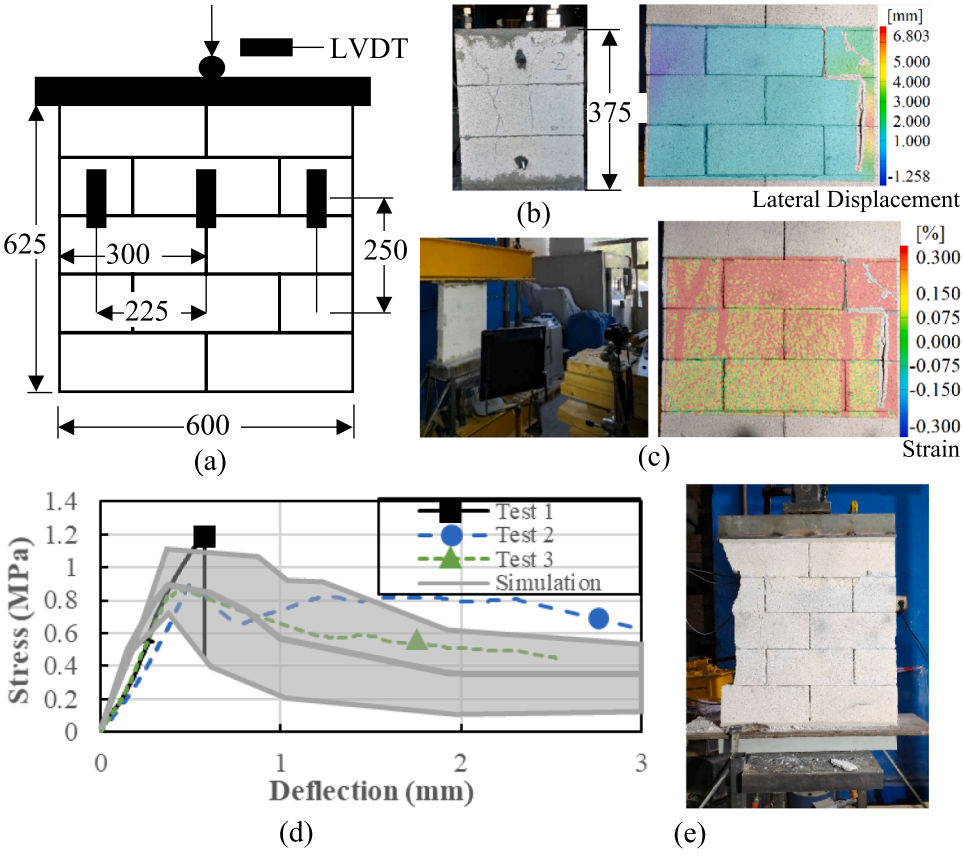

Fig. 5. (a) Dimensions and instrumentations (black marker as LVDT) of tested masonry wallets, (b) the specimen tested by Todorovic et al. [80]. (c) Test Setup and DIC results of tested specimens and corresponding (d) stress–deflection curves and (e) crack pattern obtained in experiment of a specimen.

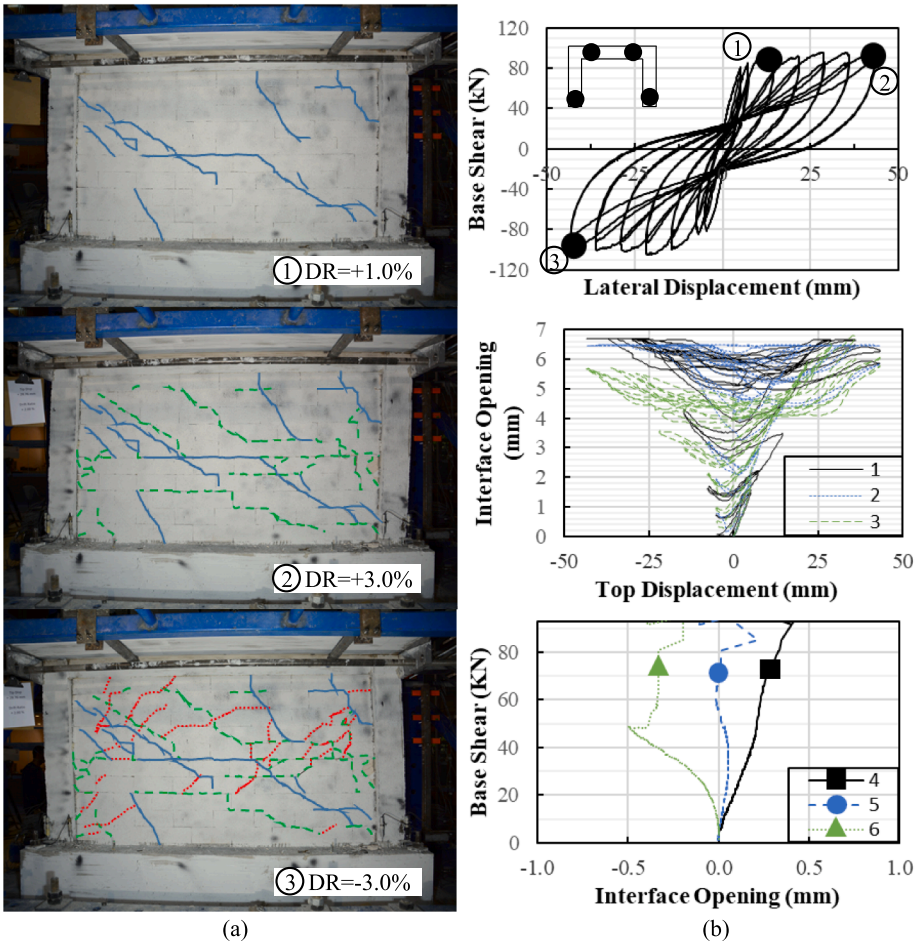

Fig. 6. (a) Cracks at different drift ratios and (b) lateral displacement-base shear and interface opening responses for corresponding LVDT labels for the specimen SP1.

example, using leveling mortar at the vertical interaction regions enabled stiffer response at the drift ratio value of about 0.5% than the specimen with foam interfaces despite the similar initial stiffness. The reason for obtaining a lower capacity of SP1 than the specimen tested by Binici et al. [66] can be attributed to different concrete strengths at the day of the experiments or mechanical properties of steel. The softer response of SP2 was observed as expected since the same frame was used after using for SP1. Moreover, the contribution of the wall with the opening on global response was negligibly small. This can be attributed to the opening in the wall of SP2, which prevents the development of a proper strut formation. The results of the Pavia tests are provided in the numerical validation section.

4. Calibration of model for AAC masonry material modeling

Calibration of the lattice model for the AAC units from two different experimental campaigns are discussed in this section. Uniaxial and diagonal compression experiments for two AAC masonry batches are simulated for different G_f and R_{max}/d values and capacity results are summarized in Table 3. While the brittle response in tension was assumed for the METU experiments, a fracture energy of 56.7 N/m was used for batch 2, the Pavia experiments, as suggested by Milanesi et al. [30]. The tension softening parameters were found by executing the flow-chart using provided tensile strength (f_{ta}), modulus of elasticity and fracture energy (G_f) values, as shown in Fig. 2. All mechanical properties of AAC masonries and corresponding tension softening parameters determined based on the procedure of explained in Section 2 and Fig. 2 are listed in Table 2.

The random values of R_{max}/d were found by matching the uniaxial compression strength of masonry with the test results (Fig. 2). The compression calibration procedure was applied and R_{max}/d was found as 0.125 for the AAC walls for both tests of batch 1 as explained in section 3. The range and mean of load deflection responses of 100 simulations, the comparisons of experimental and numerical results, and crack patterns from experiments and simulations are summarized in Fig. 5d, Table 3 and Fig. 8a. In Fig. 8, color contours denote the strain values of the lattice elements and the lines on the specimens represent the observed cracks during the tests. The experimental results appear to be in the range of 100 simulation results. On the other hand, Costa [82] performed six uniaxial compression tests for the AAC wallettes for batch 2. Three of each were tested in different orientations (vertical and horizontal, with 90 degrees rotated). The dimensions (length × width) of these two specimens were 940x1250 mm and 1000x940mm for vertical and horizontal specimens. The mean compressive strength of AAC masonries was reported as about 2.07 MPa. The same calibration procedure was performed, and R_{max} value was found as 2.0 mm for the grid size (d) of 30 mm.

The performance of the calibrated model (i.e., for R_{max}/d and G_f) was first examined with the diagonal tests. Two and seven specimens with the dimensions (length × width × thickness) of 750x750x150 mm (Fig. 8b) and 630x750x300 mm were compressed diagonally for batch 1 and batch 2, respectively [30,83]. According to ASTM E519-10 [84], two steel loading shoes were used and the length and height of bearing of loading head are determined about 150 mm and 100 mm, respectively. Thus, the top and bottom boundary nodes are restrained in both directions. The determined capacities from simulations and experiment

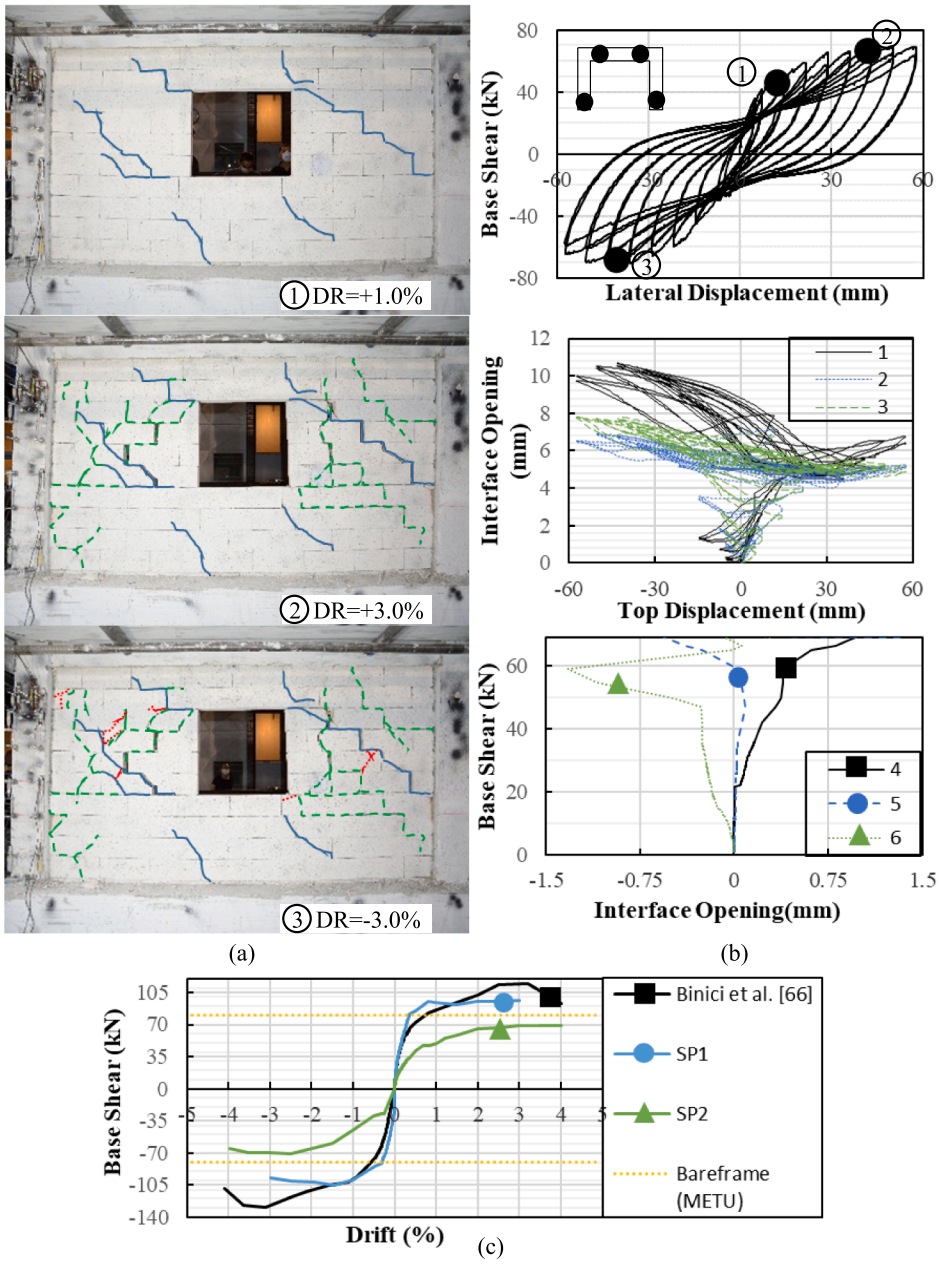

Fig. 7. (a) Cracks at different drift ratios, (b) lateral displacement-base shear and interface opening responses for corresponding LVDT labels for the specimen SP2 and (c) drift-base shear curve comparisons for bare frame and infill walls as Binici et al. [66], SP1, SP2.

Table 2
Material properties of AAC masonries.

Properties (AAC)	Batch 1 (METU)	Batch 2 (Pavia)[a]
Thickness (mm)	10	30
Modulus of Elasticity (MPa)	1000	1498
Density (kg/m^3)	350	484
Tension Strength (f_{ta}) (MPa)	0.300[b]	0.278
Compression Strength (MPa)	0.9	2.0
Fracture Energy (N/m)	(Brittle)[b]	56.7
a_1 [c]	1.50	1.50
a_2	1.51	140.00
a_3	1.52	600.00
R_{max}/d	0.125	0.067

[a] Values were taken from Milanesi et al.[30]
[b] Calibrated values from tests
[c] Fracture energy parameters were found for d = 5 mm

results and crack patterns can be found in Table 3 and Fig. 8b.

While the capacity estimation for G_f and R_{max}/d values of 56.7 N/m and 0.067, respectively, coincides with the test results for batch 2, capacity results are found slightly lower than expected for batch 1. The reason may be partly attributed to the limited (two) number of experiments. Using a lower randomness value and a higher tension softening increases the uniaxial and diagonal compression capacity. The unique combination of R_{max}/d and G_f should be determined to employ sufficiently accurate capacity estimations for both diagonal and uniaxial tests. Thus, in the case G_f value is not available, diagonal test results additional to uniaxial compression test results can be used to calibrate both values.

Based on these calibrations and validations at the material level, the G_f , a_1 , a_2 a_3 and R_{max}/d values were established for concrete and masonry as shown in Tables 1,2.

Table 3
Results for AAC masonry diagonal and uniaxial compression experiments and simulations.

Results (MPa)	Batch 1 (METU)			Batch 2 (Pavia)			
	Uniaxial Compression Test						
	Exp	Simulation (d = 25 mm)		Exp	Simulation (d = 30 mm)		
		Brittle, $\frac{R_{max}}{d} = 0.125$			Gf = 56.7 $\frac{R_{max}}{d} = 0.067$	Brittle $\frac{R_{max}}{d} = 0.05$	Gf = 56.7 $\frac{R_{max}}{d} = 0.05$
		Todorovic et al. [80]	In this Study				
Number	8	100	100	6	100	100	100
Min.	0.87	0.65	0.70	1.98	1.70	1.39	1.93
Max.	1.20	1.20	1.13	2.25	2.50	2.21	2.88
Mean	0.98	0.92	0.90	2.07	2.04	1.84	2.29
Standard Deviation	0.10	0.11	0.09	0.10	0.16	0.15	0.16
Results (kN)	**Diagonal Test**						
	Exp	**Simulation (d = 20 mm)**		**Exp**	**Simulation (d = 30 mm)**		
Number	2	100		7	100	100	100
Min.	33.11	23.94		91.06	90.48	54.83	103.76
Max.	48.85	32.80		146.47	150.36	107.58	162.05
Mean	40.98	25.47		114.56	111.32	71.88	131.74
Standard Deviation	–	1.18		18.98	12.97	13.09	13.65

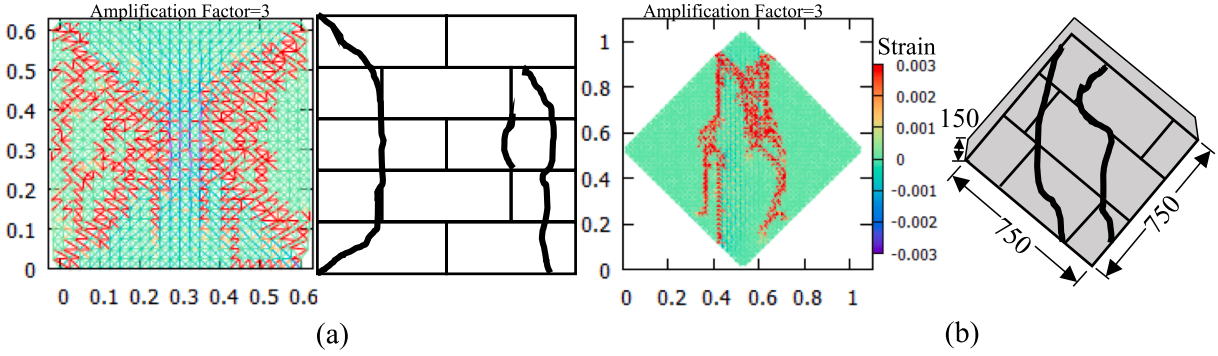

Fig. 8. Cracks in (a) uniaxial compression and (b) diagonal compression tests from experiments (representative) and simulations of batch 1.

5. Validations

Simulations of four AAC infilled portal frames, discussed in Section 3, labeled as Pavia Test and METU Tests, consisting of the tests Binici et al. [66], SP1, SP2 and Penna and Calvi [67] are conducted with the lattice models described in Section 2. Dimensions of infill specimens and mechanical properties are given in Fig. 3, Fig. 4, Table 1, and Table 2. Various interaction types of frames and walls such that 1 cm and 2 cm gap with foam or leveling mortar were modeled with special interaction elements explained in Section 2. E_i , m_t and n values for foam elements were selected as 2, 50 and 10, respectively. The bottoms of both columns were fixed. On the other hand, the bottom of the wall was released in the lateral direction due to the low shear resistance of mortar in that place. The lateral load was applied as a uniformly distributed load by using PID control to avoid stress localization after applying axial load on the related top nodes [42–43]. The imposed lateral displacement was increased monotonically. The grid sizes were adjusted in order to place the longitudinal reinforcements at their exact locations. The lines on the estimated cracking images of infill walls at the end of the simulation in the figures represent the observed cracks during the tests.

5.1. Bare and infilled frame [47]

The single-bay and single-story half-scale portal bare frame with planar dimension of 2500x1500 was tested in Middle East Technical University's laboratory by Binici et al. [66]. This specimen was used as the first validation experiment. The specimen properties, dimensions, and the details of the reinforcement used in test specimens are presented in Table 1 and Fig. 4a. Details are provided in Section 3. Reported values, if available, were used for the simulation, while corresponding standards were used for the parameters that were not reported. In the models, three types of elements were used for steel, concrete, and bond, as mentioned in section 2.

The load–deflection curve from the simulations is shown in Fig. 9a. Grid size (d) was chosen as 20 mm. Two different α values, 0.7 and the value found by Eq. (1) as 0.3, were chosen to investigate the effect of residual bond strength value on the global response. The initial stiffness from the simulation and experiments were close to each other for the α value of 0.7. Also, the base shear simulation resembled the envelope of the experimental response until the displacement value of about 10 mm. However, the capacity was overestimated; the simulated lateral load-carrying capacity was 100 kN, versus an experimental capacity of 83 kN. Spalling was observed during the experiment after a 3.0% drift ratio at the column base [66] (Fig. 9b). Fig. 9b represents the strain values of concrete and steel elements near the end of the simulation. With a uniform surface grid, the concrete element on the outer part of the compression edge of the column sustained high forces due to linear response in compression. On the other hand, with an α value of 0.3, as found by Eq. (1), the experimental load–deflection curve is sufficiently accurately duplicated (Fig. 9c). Moreover, cover spalling following by rebar buckling was exhibited.

The grid sizes for infilled frame specimens tested at METU were selected as 20 mm. The foam elements were placed on all interaction regions between columns, beam, and wall. The lateral load–deflection curve is shown in Fig. 10a. Initial stiffness and capacity were estimated with sufficient accuracy. The capacity was reached at a smaller

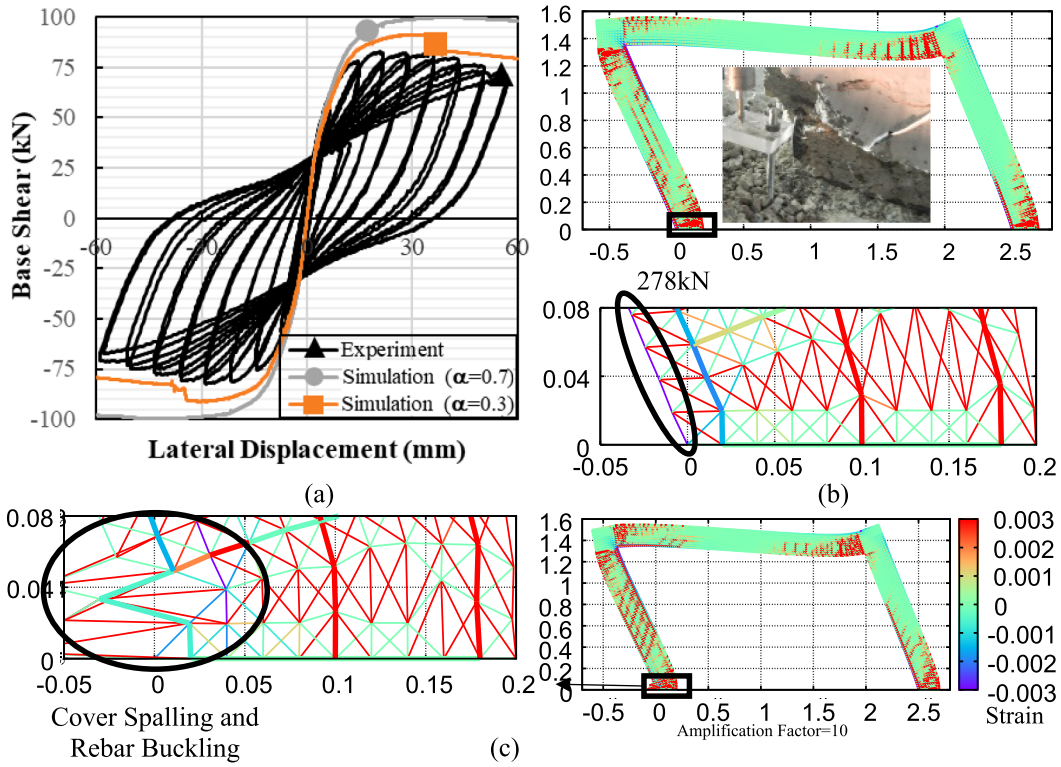

Fig. 9. Experiment and simulation results of the METU bare frame [66]: (a) Base shear – lateral displacement curve, cracks in the simulation for the frame and zoomed section of (b) $\alpha = 0.7$ and (c) $\alpha = 0.3$ (found from Eq. (1)).

displacement demand than the experimental measurement. Also, the capacity loss was simulated earlier than observed experimentally. The reason can be attributed to the absence of the cyclic loading in the simulation and improper strut formation in the positive direction in the experiment. However, the residual strength capacity was estimated close to the experimental result at the displacement value of about 55 mm and, also, the global response in the simulation was in between the positive and negative responses of the experiment.

The cracks in the experiment at positive and negative drift ratio values of 3.0% and 3.5%, respectively and in the simulation at 1.32% and 4.00% lateral drift ratios are compared in Fig. 10b,c. Diagonal struts and corresponding splitting cracks were visible in the experiment and also observed in the simulations. Also, the corner cracks reported in the test were also simulated by correctly representing the contact behavior.

5.2. Infilled frames in this study

SP1 and SP2 explained in Section 2 were simulated with the proposed lattice model. The grid sizes for specimens were chosen as 20 mm. The foam elements were placed at only the top of the wall. Brittle AAC elements were placed at the left and right interaction regions.

Lateral load–deflection curves from simulation and experiment of SP1 are shown in Fig. 11a. Initial stiffness, strength, and load-deformation response were estimated with reasonable agreement, along with the deformation capacity, when the simulation results were compared with the envelope response of experiment. Moreover, interface responses at the ends of the beam from simulation and experiment are shown in Fig. 11a. LVDT numbering corresponds the measurement regions proposed in Fig. 3a. The results proposed from the simulation at the related location of LVDTs are in good agreement with the experimental results based on the estimation of interaction response. Major strain distribution in addition to the displacements in lateral direction of nodes observed in DIC from the experiment and cracks in simulation at 1.39% and 2.92% lateral drift ratios are shown of Fig. 11b. In the figure, cracks observed in the experiment as shown in Fig. 6a are sketched on the simulation result at 42 mm lateral displacement. The estimated crack locations were in good agreement with the test results. The DIC results indicated the partitioning of horizontal wall segments. The lateral movements between segments were successfully captured with the proposed lattice model.

It should be clarified that after using the undamaged frame for SP1 until a 3.0% drift ratio, the same but the damaged frame was used for SP2, as mentioned in Section 3. After the SP1 experiment was conducted, the wall was removed, and a new AAC wall with the opening was placed in the damaged frame to prepare the SP2. In order to simulate the damaged frame, the simulated cumulated damage after unloading specimen SP1 is recorded and input as a pre-damage of the frame of specimen SP2. Fully elastic AAC elements were assigned at the region of the lintel. The load–deflection curve of SP2 is shown in Fig. 12a. Simulations of the initial stiffness and subsequent softening of the specimen with the damaged frame were accurate. The lateral strength was slightly overestimated, beyond the peak displacement of about 40 mm. Furthermore, comparisons of the interaction region are shown in Fig. 12a, which show an accurate interface response. The cracks in simulation at 1.60% and 4.00% lateral drift ratios are shown in Fig. 12b with representative experimental cracking lines corresponding the results proposed in Fig. 7a. There is a reasonable agreement in the main crack directions while additional micro-cracks were noted in the simulation. Two struts in the wall around the opening were simulated. The same observation was also found in the experiments as shown in Fig. 7a.

5.3. Pavia test

Finally, the AAC infilled wall tested by Penna and Calvi [67] was simulated with a grid size value of 30 mm. Here, no gaps between concrete and wall are present, as mentioned in section 3. The interface mortar was modeled with the same mechanical properties of the brittle AAC elements with the reported and calibrated tensile strength value of

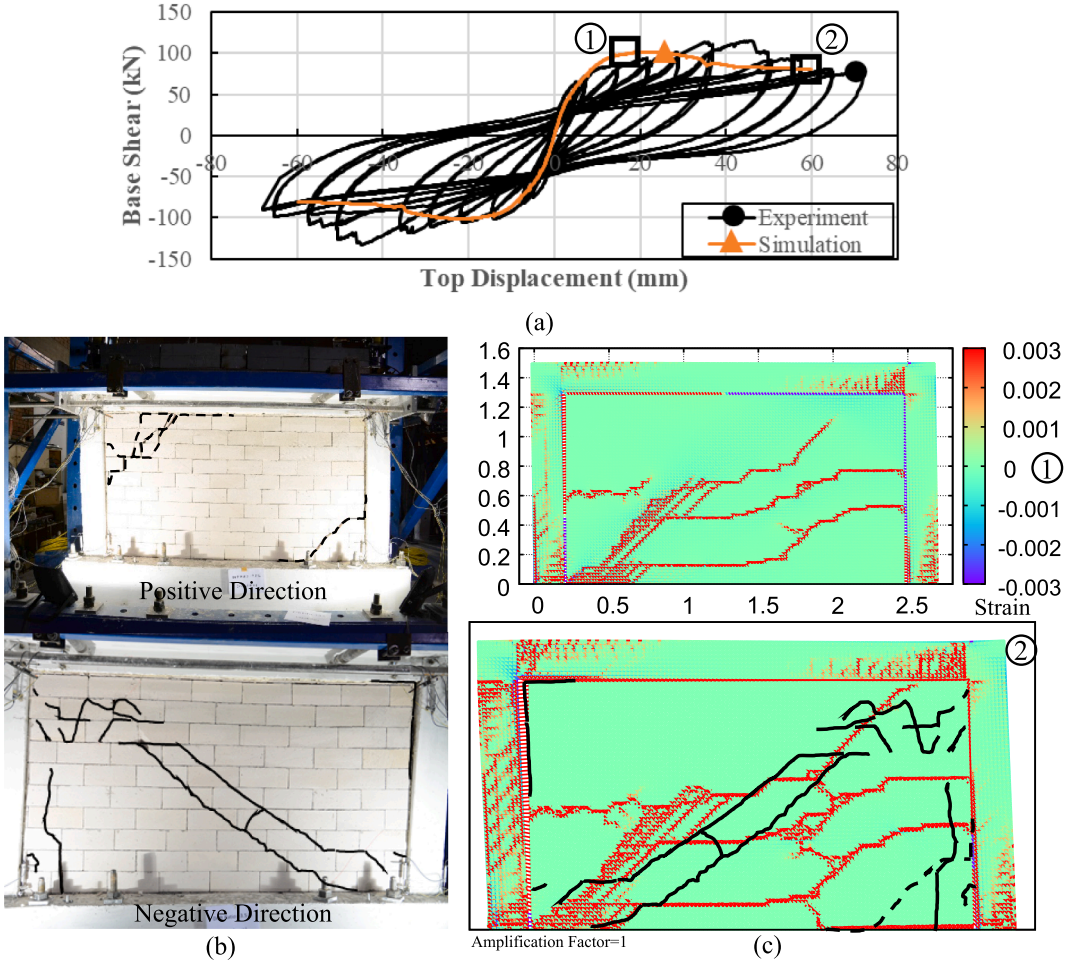

Fig. 10. Experiment and simulation results of infill test [66]: (a) base shear – top displacement responses, and cracks (b) in experiment at positive (3.0% drift ratio) and negative (3.5% drift ratio) directions, (c) in simulation at 1.32% and 4.00% lateral drift ratios with observed experimental cracks.

0.1 MPa by Milanesi et al. [30]. Lateral load-top deflection curve comparisons of two different grid perturbation instances with calibrated R_{max}/d values and experiment results are provided in Fig. 13a. The initial stiffness is in perfect agreement with the test results. The first softening region at the displacement value of about 5 mm was captured in the simulation with a slight strength degradation. A higher capacity was simulated after a displacement of about 10 mm in the positive direction. At 20 mm, a considerable strength degradation was observed in the simulation, and the capacity was close to the test results. Besides, the effect of using a different realization of node perturbation, with the same R_{max}/d, is insignificant.

The crack pattern estimation with the lattice model is shown in Fig. 13b. In the figure, lines on images of strain distribution in the simulation represent the cracks observed at the near end of the experiment at positive and negative lateral directions. The two simulation results generally agree with the observation of Penna and Calvi [67]. Diagonal struts were observed to be starting from the left top corner extending towards the right bottom of the wall. The splitting cracks were also captured in the simulations. Although the two simulations result in marginal differences in the load–deflection responses, minor differences for the crack predictions were observed.

The envelope curves shown in Figs. 9-13 are within 5% in terms of strength estimations except Pavia test. In the Pavia test, the strength is overestimated by 25 to 35% in the positive and 6 to 13% in the negative direction. This result can be attributed to the variation of material strength in the test or small deviations of longitudinal bar placement. In order to obtain fully conservative results, use of characteristic strength values instead of mean strength can be a viable approach as usually used in design.

6. Parametric study

The local behavior affects the global response of the infilled frames, such as reduction of clear high of the column or increasing shear demands with diagonal struts in full contact with the frame. The contact length represents the connection length of the diagonal strut at the column part. Considerable analytical formulations have been provided for estimation the contact length and strut width, by many researchers and corresponding codes. Asteris et al. [29] and Morandi et al. [85] proposed further details about the simplified approaches. In this study, contact length results estimated with the proposed lattice model were compared with results found with formulations proposed by FEMA-306 [86] as popular formulation and Pauley and Priestley [87] conservative approach, for the infill walls with different length scale (L/H) values and interface properties. FEMA-306 estimates the width on the basis of experimental and analytical data by including slenderness of infill (λ). The effective width of the strut (b_w is found with the following equation;

$$b_w = 0.175 d_w (\lambda h)^{-0.4} \tag{3}$$

Where d_w is diagonal length of infill wall, and h is column centerline height of the columns. On the other hand Pauley and Priestley [87] assumes one quarter of diagonal length of infill wall (d_w) as the strut width (b_w). In both approaches, strut thickness is assumed same as the wall thickness. L/H values were chosen as 1.00, 1.57 (Pavia Test), 1.79

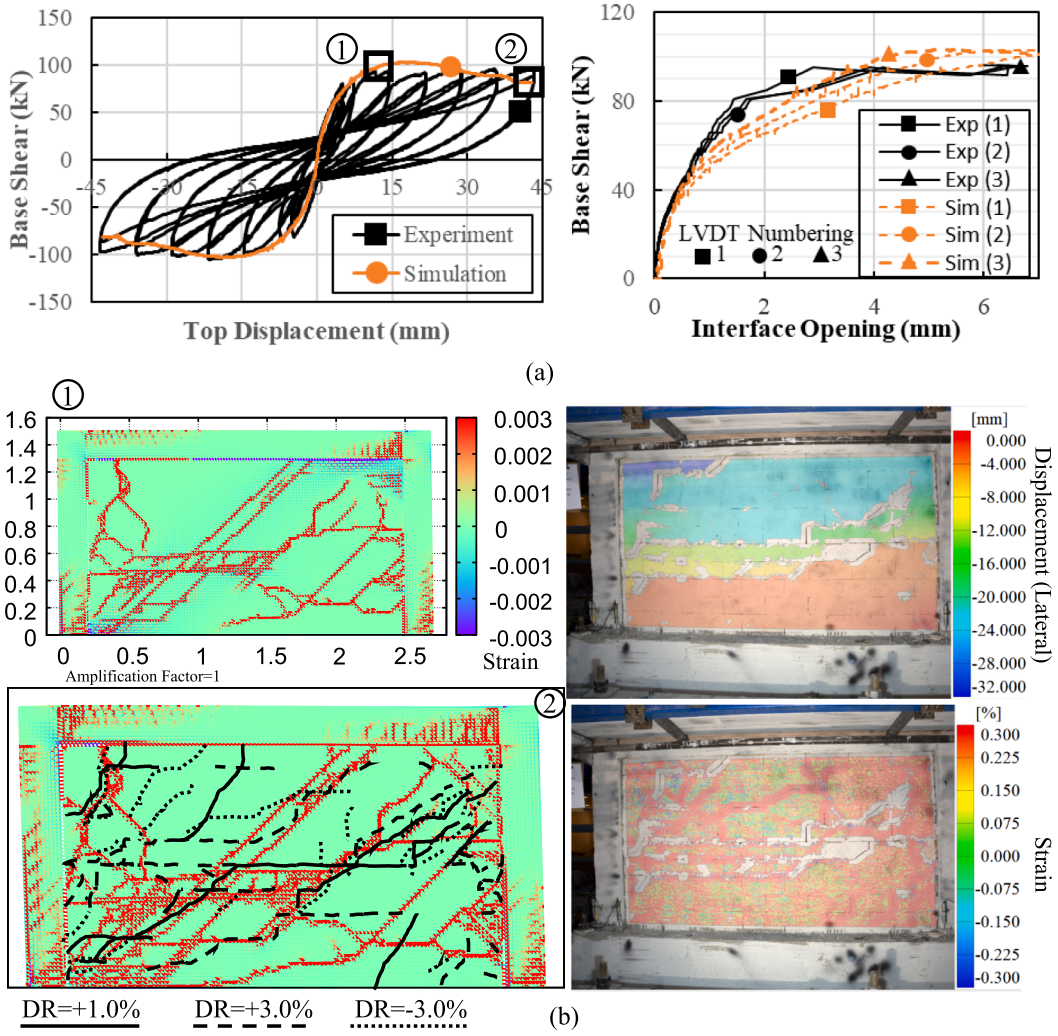

Fig. 11. Experiment and simulation results of infill test, SP1: (a) Base shear – top displacement responses and interface openings of corresponding LVDTs and (b) cracks in simulation at 1.39% and 2.92% lateral drift ratios with observed experimental cracks at different drift ratios and DIC results including lateral displacement and strain distributions.

(SP1), and 3.00 and interface properties were similar to infill walls of SP1 (only upper side foam), Pavia Test [67] (no foam) and Binici et al. [66] (all sides foam). Contact length is assumed as the vertical component of equivalent strut width. The variation of contact lengths through the lateral displacement demands are shown in Fig. 14.

The compression regions were observed from the top of the loaded column and from the bottom of the pulled column, as shown in Section 5. The contact length was calculated by monitoring the relative distance of the element nodes in the interaction region. For low inter-story drift ratios, the results are close to the results of both simplified approaches. Complicated behavior is obtained after cracking and the contact length at loaded column increased, although not monotonically, with an increasing drift ratio. Different types of interface region affect the contact length behavior significantly, as well. This phenomenon is not addressed in the existing simple strut models. It can be observed that as the aspect ratio of the infill wall increases the estimation of the models tend to be closer to the simplified strut widths. The estimated contact length in strut top and bottom are different.

7. Conclusion

A two-dimensional mesoscale truss-based lattice modeling approach was proposed AAC infilled frames for the first time in the literature. A compression calibration methodology described in Aydin et al. [43] was modified for wall elements, by using uniaxial diagonal compression tests of masonries. Overall load–deflection responses and crack patterns of masonry simulations are in reasonable agreement with the test results. Two single-bay, single-story half-scaled AAC infilled portal frames experiments were carried out to investigate the interaction of AAC wall and frame with and without opening in the wall, and to achieve validation benchmarks for the proposed model. Two additional AAC infilled frame tests were used from the literature for the same purpose. The AAC infilled frame experiment results show that interaction properties affect the global response based on rigidity and strength of infill walls.

The RC frame tested by Binici et al. [66] was simulated with the proposed lattice approach. Simulations with a different residual bond strength showed that the effect of the residual bond strength on the lateral load-top displacement response was significant. A residual bond strength was selected, which also lead to reasonable crack predictions. Also, cover spalling and rebar buckling, as reported by Binici et al. [66], was simulated at a drift ratio of about 3.0%.

Four infill walls with different interaction region properties were modeled to validate the proposed numerical approach for AAC infilled frames. Load-deflection and crack propagation gave close simulations of the experimental results. The maximum difference between the simulated and experimental lateral load capacity was found for the Pavia test [67] (13%). Results from the simulations using different realizations of the same node perturbance R_{max}/d were relatively close. The crack

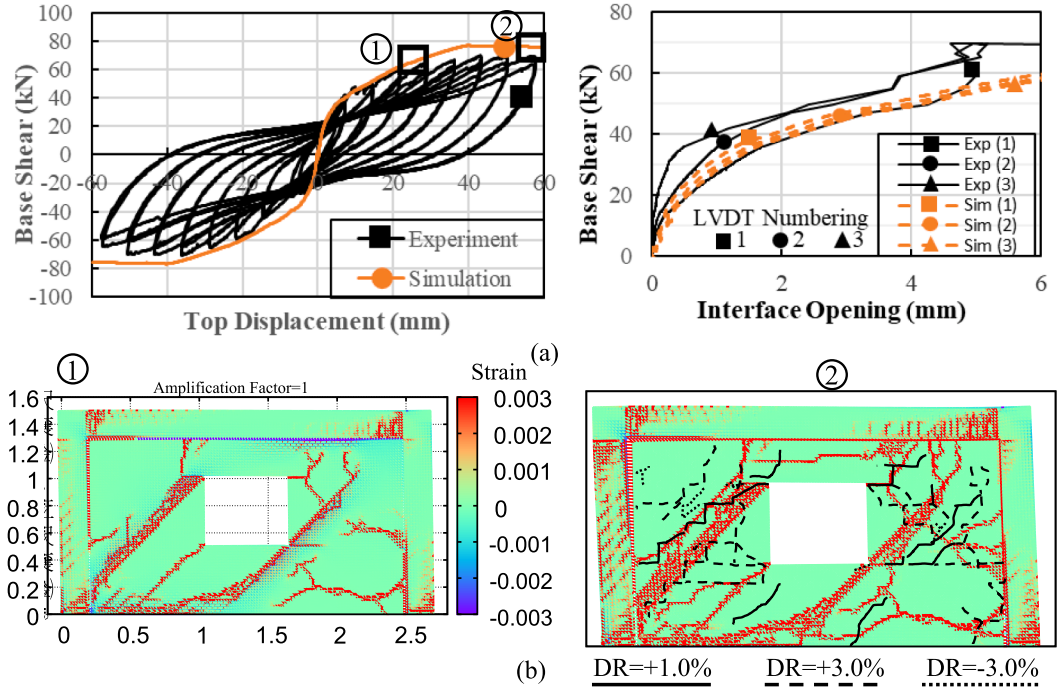

Fig. 12. Experiment and simulation results of infill test, SP2: (a) Base shear – top displacement responses and interface openings of corresponding LVDTs and (b) cracks in simulation at 1.60% and 4.00% lateral drift ratios with observed experimental cracks at different drift ratios.

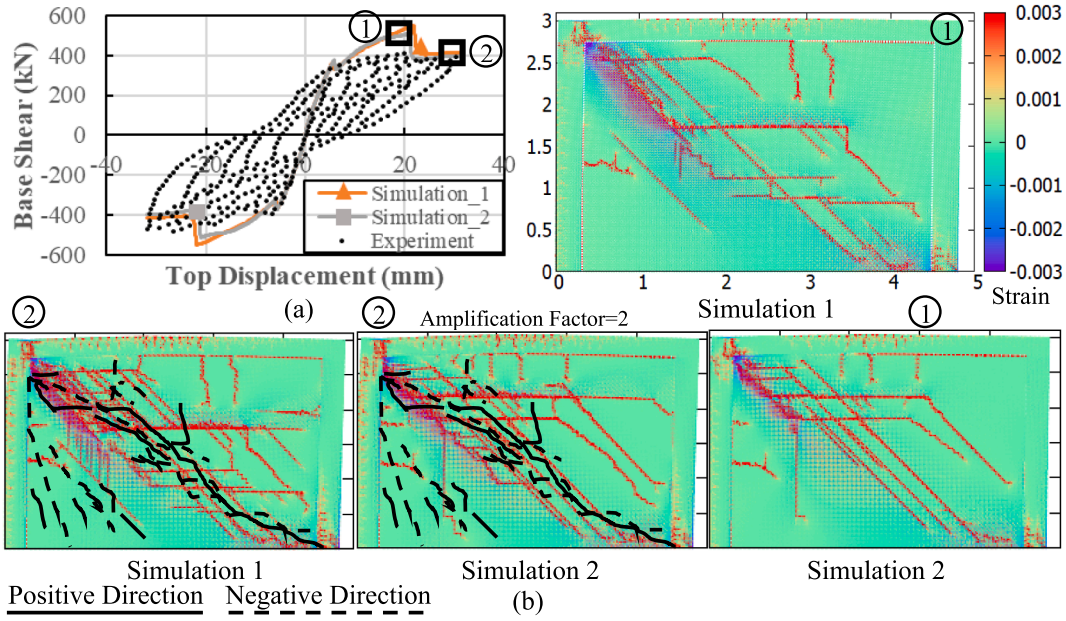

Fig. 13. Experiment and simulation results of Pavia infill test [67], SP2: (a) Base shear – top displacement curve and (b) cracks for two simulations at 0.66% and 1.11% lateral drift ratios with observed experimental cracks at directions.

patterns were simulated in good agreement with the test results. Diagonal struts and corresponding splitting cracks, and two struts due to an opening in the wall, were simulated with the proposed model. Using special interface truss elements, the interaction between walls and frames was simulated realistically. In a parametric study the evolution of the contact length was simulated for different aspect ratios and interface region properties of the walls. The results were presented and compared with widely used simplified approaches. The infill wall-frame contact length depends on lateral deformation demands and interaction properties significantly.

In conclusion, it appears that the lattice approach provides a practical and efficient model to simulate infill walls and their components. Both global and local behavior are simulated well. The modeling approach, including an extended calibration procedure, can be consistently applied for a range of experiments, including AAC masonries, RC frame structures and AAC infilled frames. Application of the lattice models in building design is a challenging issue due to high computational efforts. However, lattice models can be employed within a substructure framework where the building inter-story demands can be imposed on the one bay one-story infilled RC frame to estimate the

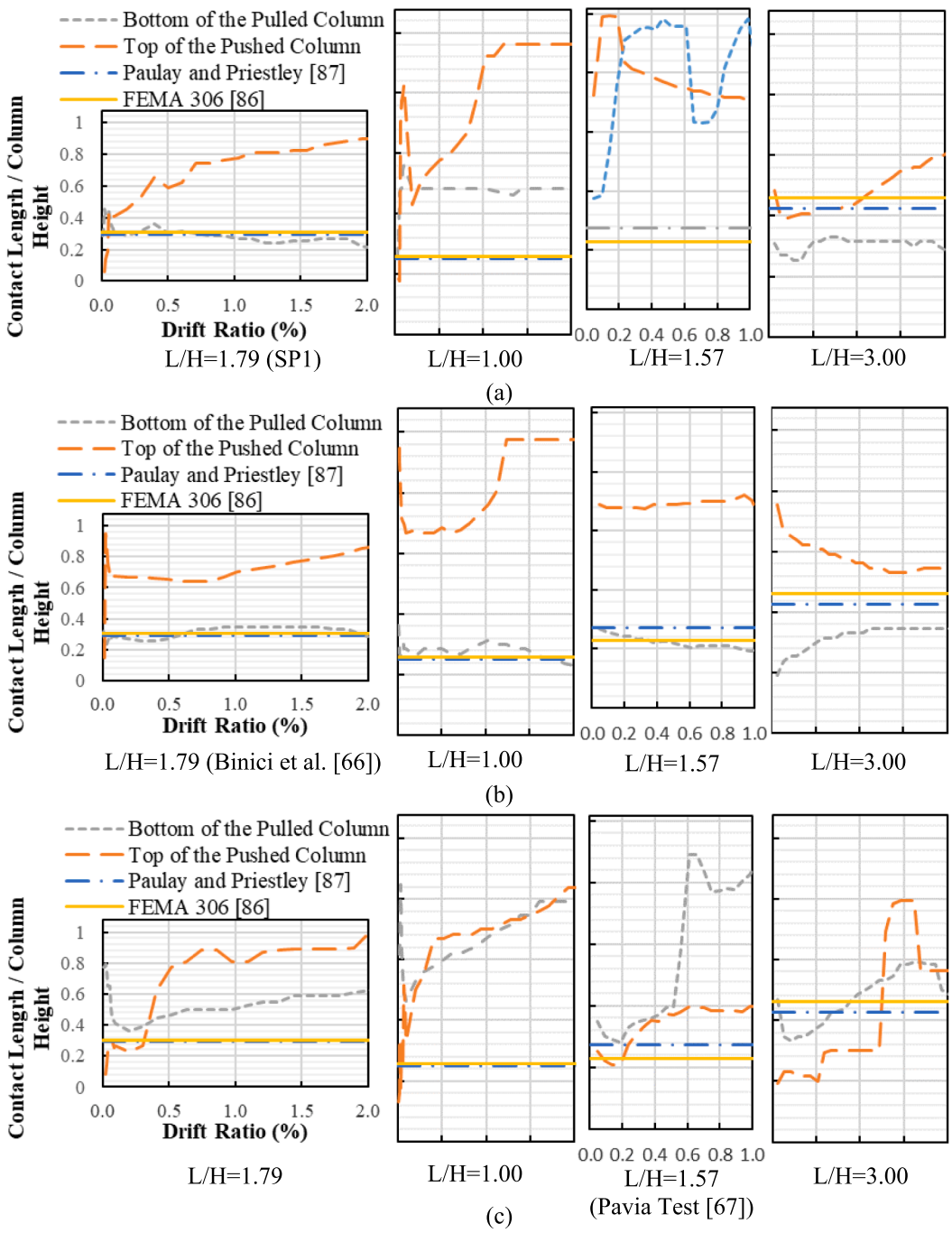

Fig. 14. Contact length in columns and drift ratio curves for different length scales (L/H) and interface properties of (a) SP1 (only upper side foam), (b) Binici et al. [66] (all sides foam), (c) Pavia Test [67] (no foam).

damage limit state of infill walls. A complete crack formation in an infill wall estimated with the lattice model can be considered as high damage whereas limited cracking can be considered as low damage. Alternatively, the findings on infill wall frame contact length can be used to create classical truss based compression only strut models. Further work is needed for establishing design oriented lattice based approaches.

CRediT authorship contribution statement

Beyazit B. Aydin: Writing – original draft, Software, Validation, Investigation, Visualization. **Baris Binici:** Methodology, Conceptualization, Validation, Writing – review & editing. **Max A.N. Hendriks:** Methodology, Validation, Writing – review & editing. **Kagan Tuncay:** Software, Methodology.

Declaration of Competing Interest

The authors declare that they have no known competing financial interests or personal relationships that could have appeared to influence the work reported in this paper.

Acknowledgements

This research was supported by the Scientific and Technological Research Council of Turkey (TUBITAK), 2214-A, application number: 1059B141900037.

References

[1] Penna A, Morandi P, Rota M, Manzini CF, da Porto F, Magenes G. Performance of masonry buildings during the Emilia 2012 earthquake. Bull Earthq Eng 2014;12(5):2255–73.
[2] Braga F, Manfredi V, Masi A, Salvatori A, Vona M. Performance of non-structural elements in RC buildings during the L'Aquila, 2009 earthquake. Bull Earthq Eng 2011;9(1):307–24.
[3] Vicente RS, Rodrigues H, Varum H, Costa A, Mendes da Silva JAR. Performance of masonry enclosure walls: lessons learned from recent earthquakes. Earthq Eng Eng Vib 2012;11(1):23–34.
[4] Ricci P, De Luca F, Verderame GM. 6th April 2009 L'Aquila earthquake, Italy: reinforced concrete building performance. Bull Earthq Eng 2011;9(1):285–305.
[5] Binici B, Yakut A, Gülkan P. Van Depremine Yerleşimler Açısından Bakış ve Tavsiyeler. Bilim ve Teknik Dergisi 2012;(January):26–31.
[6] Polyakov SV. Investigation of the Strength and of the Deformational Characteristics of Masonry Filler Walls and Facing on Framed Structures. Construction Industry Institute 1950;No.3.
[7] Klingner RE, Infilled BVV. frames in earthquake-resistant construction. Report EERC/76-32, Earthquake Engineering Research Center. Berkeley, CA, USA: University of California; 1976.
[8] Smith BS. Behaviour of Square Infilled Frames. ASCE Journal of Structural Division 1966;92 ST1:381-403 February.
[9] Asteris PG, Kakaletsis DJ, Chrysostomou CZ, Smyrou EE. Failure modes of infilled frames. Electronic Journal of Structural Engineering 2011;11(1):11–2011.
[10] Alwashali H, Sen D, Jin K, Maeda M. Experimental investigation of influences of several parameters on seismic capacity of masonry infilled reinforced concrete frame. Eng Struct 2019;189:11–24.
[11] Asteris PG. Lateral stiffness of brick masonry infilled plane frames. J Constr Steel Res 2003;129:1071–9.
[12] Papia M, Cavaleri L, Fossetti M. Infilled frames: developments in the evaluation of the stiffening effect of infills. Structural Engineering and Mechanics 2003;16(6):675–93.
[13] Cavaleri L, Fossetti M, Papia M. Modeling of out-of-plane behavior of masonry walls. J Struct Eng 2009;135(12):1522–32.
[14] Mohebkhah A, Tasnimi AA. Distinct element modeling of masonry-infilled steel frames with openings. Open Construction and Building Technology Journal 2012;6:42–9.
[15] Nicola T, Leandro C, Guido C, Enrico S. Masonry infilled frame structures : state-of-the-art review of numerical modelling. Earthquakes Struct 2015;8(1):225–51.
[16] Polyakov SV. On the interaction between masonry filler walls and enclosing frame when loaded in the plane of the wall. Transl Earthq Eng 1960;2(3):36–42.
[17] Chrysostomou CZ, Gergely P, Abel JF. A six-strut model for nonlinear dynamic analysis of steel infilled frames. Int J Struct Stab Dyn 2002;02(03):335–53.
[18] El-Dakhakhni WW, Elgaaly M, Hamid AA. Three-strut model for concrete masonry-infilled steel frames. J Struct Eng 2003;129(2):177–85.
[19] Galli M. Evaluation of the seismic response of existing R.C frame buildings with masonry infill. MSc Dissertation. Pavia, Italy: ROSE School; 2006.
[20] Amato G, Cavaleri L, Fossetti M, Papia M. Infilled frames: influence of vertical loads on the equivalent diagonal strut model. In: The 14th world conference on earthquake engineering, Beijing, China, 2008.
[21] Kadysiewski S, Mosalam KM. Modeling of unreinforced masonry infill walls considering in-plane and out-of-plane interaction PEER Report 2008/ 102. Berkeley: University of California; January 2009.
[22] Federal Emergency Management Agency. FEMA. Prestandard and commentary for the seismic rehabilitation of buildings. Report no. FEMA 356. Washington (DC): FEMA; 2000.
[23] Masonry Standards Joint Committee. MSJC. Building code requirements and specification for masonry structures and related commentaries. TMS 602-11/ACI 530.1-11/ASCE 6-11. Farmington Hills (MI, USA): American Concrete Institute; 2011.
[24] Canadian Concrete Masonry Producers Association. CCMPA. Seismic design guide for masonry buildings. Toronto (Canada): CCMPA; 2009.
[25] Turgay T, Durmus MC, Binici B, Ozcebe G. Evaluation of the predictive models for stiffness, strength, and deformation capacity of RC frames with masonry infill walls. J Struct Eng 2014;140(10):06014003. https://doi.org/10.1061/(ASCE)ST.1943-541X.0001069.
[26] Mehrabi AB, Shing PB. Finite element modelling of masonry-infilled RC frames. J Struct Eng ASCE 1997;5:604–13.
[27] Mosalam KM, White RN, Gergely P. Static response of infilled frames using quasi-static experimentation. J Struct Eng 1997;123(11):1462–4169.
[28] Sutcliffe DJ, Yu HS, Page AW. Lower bound limit analysis of unreinforced masonry shear walls. Comput Struct 2001;79(14):1295–312.
[29] Asteris PG, Cotsovos DM, Chrysostomou CZ, Mohebkhah A, Al-Chaar GK. Mathematical micromodeling of infilled frames: state of the art. Eng Struct 2013;56:1905–21.
[30] Milanesi RR, Morandi P, Magenes G. Local effects on RC frames induced by AAC masonry infills through FEM simulation of in-plane tests. Bull Earthq Eng 2018;16(9):4053–80.
[31] Fenerci A, Binici B, Ezzatfar P, Canbay E, Ozcebe G. The effect of infill walls on the seismic behavior of boundary columns in RC frames. Earthq. Struct. 2016;10(3):539–62.
[32] Lotfi HR, Shing PB. Interface model applied to fracture of masonry structures. J Struct Eng 1994;120(1):63–80.
[33] Giambanco G, Di Gati L. A cohesive interface model for the structural mechanics of block masonry. Mech Res Commun 1997;24(5):503–12.
[34] Gambarotta L, Lagomarsino S. Damage models for the seismic response of brick masonry shear walls. Part I. The mortar joint model and its applications. Earthquake Eng Struct Dyn J 1997;26(4):423–39.
[35] Oliveira DV, Lourenço PB. Implementation and validation of a constitutive model for the cyclic behaviour of interface elements. Comput Struct 2004;82(17-19):1451–61.
[36] Alfano G, Sacco E. Combining interface damage and friction in a cohesive-zone model. Int J Numer Meth Eng 2006;68(5):542–82.
[37] Fouchal F, Lebon F, Titeux I. Contribution to the modelling of interfaces in masonry construction. Constr Build Mater 2009;23(6):2428–41.
[38] Pari M, Van de Graaf AV, Hendriks MAN, Rots JG. A multi-surface interface model for sequentially linear methods to analyse masonry structures. Eng Struct 2021;238:112123. https://doi.org/10.1016/j.engstruct.2021.112123.
[39] Itasca consulting group. Inc. UDEC- Universal distinct element code. Version 4.0-User's manual. Minneapolis (MN, USA) 2004.
[40] Negro P, Colombo A. Irregularities induced by nonstructural masonry panels in framed buildings. Eng Struct 1997;19(7):576–85.
[41] Aydin BB, Tuncay K, Binici B. Overlapping lattice modeling for concrete fracture simulations using sequentially linear analysis. Structural Concrete 2018;19(2):568–81.
[42] Aydin BB, Tuncay K, Binici B. Simulation of reinforced concrete member response using lattice model. Journal of Structural Engineering ASCE 2019;145(9):04019091. https://doi.org/10.1061/(ASCE)ST.1943-541X.0002381.
[43] Aydin BB, Binici B, Tuncay K. Lattice simulation of concrete compressive behaviour as indirect tension failure. Mag Concr Res 2021;73(8):394–409.
[44] Kawai T. New discrete models and their application to seismic response analysis of structures. Nuclear Engng. Design 1978;48:207–29.
[45] Zubelewicz A, Bažant ZP. Interface element modeling of fracture in aggregate composites. J Eng Mech 1987;113(11):1619–30.
[46] Griffiths DV, Mustoe GGW. Modelling of elastic continua using a grillage of structural elements based on discrete element concepts. Int J Numer Meth Eng 2001;50(7):1759–75.
[47] Cusatis G, Bažant ZP, Cedolin L. Confinement-shear lattice model for concrete damage in tension and compression. I. theory. J Eng Mech – ASCE 2003;129(12):1439–48.
[48] Lale E, Rezakhani R, Alnaggar M, Cusatis G. Homogenization coarse graining (HCG) of the lattice discrete particle model (LDPM) for the analysis of reinforced concrete structures. Eng Fract Mech 2018;197:259–77.
[49] Alnaggar M, Pelessone D, Cusatis G. Lattice discrete particle modeling of reinforced concrete flexural behavior. J Struct Eng 2019;145(1):04018231. https://doi.org/10.1061/(ASCE)ST.1943-541X.0002230.
[50] Lilliu G, van Mier JGM. 3D lattice type fracture model for concrete. Eng Fract Mech. 2003;70(7-8):927–41.
[51] Karihaloo BL, Shao PF, Xiao QZ. Lattice modelling of the failure of particle composites. Eng Fract Mech 2003;70(17):2385–406.
[52] Liu JX, Deng SC, Zhang J, Liang NG. Lattice type of fracture model for concrete. Theor Appl Fract Mech 2007;48(3):269–84.
[53] Aziz A. Simulation of fracture of concrete using micropolar peridynamics. MSc dissertation. New Mexico, USA: the University of New Mexico; 2014.
[54] Kilic B, Agwai A, Madenci E. Peridynamic theory for progressive damage prediction in center-cracked composite laminates. Compos Struct 2009;90(2):141–51.
[55] Oterkus E, Madenci E, Weckner O, Silling S, Bogert P, Tessler A. Combined finite element and peridynamic analyses for predicting failure in a stiffened composite curved panel with a central slot. Compos Struct 2012;94(3):839–50.
[56] Van Mier JGM. Concrete Fracture a Multiscale Approach. Boca Raton, Florida, USA: CRC Press; 2013.
[57] Birck G, Iturrioz I, Lacidogna G, Carpinteri A. Damage process in heterogeneous materials analyzed by a lattice model simulation. Eng Fail Anal 2016;70:157–76.
[58] Cusatis G, Pelessone D, Mencarelli A. Lattice discrete particle model (LDPM) for failure behavior of concrete. I: Theory. Cem Concr Compos 2011;33(9):881–90.
[59] Cusatis G, Mencarelli A, Pelessone D, Baylot J. Lattice discrete particle model (LDPM) for failure behavior of concrete. II: Calibration and validation. Cem Concr Compos 2011;33(9):891–905.
[60] Pathirage M, Bousikhane F, D'Ambrosia M, Alnaggar M, Cusatis G. Effect of alkali silica reaction on the mechanical properties of aging mortar bars: Experiments and numerical modeling. Int J Damage Mech 2019;28(2):291–322.
[61] Han L, Pathirage M, Akono AT, Cusatis G. Lattice discrete particle modeling of size effect in slab scratch tests. Journal of Applied Mechanics 2021;88(2):021009.
[62] Angiolilli M, Gregori A, Pathirage M, Cusatis G. Fiber Reinforced Cementitious Matrix (FRCM) for strengthening historical stone masonry structures: Experiments and computations. Eng Struct 2020;224:111102. https://doi.org/10.1016/j.engstruct.2020.111102.
[63] Angiolilli M, Pathirage M, Gregori A, Cusatis G. Lattice discrete particle model for the simulation of irregular stone masonry. J Struct Eng 2021;147(9):04021123. https://doi.org/10.1061/(ASCE)ST.1943-541X.0003093.
[64] Mercuri M, Pathirage M, Gregori A, Cusatis G. Computational modeling of the out-of-plane behavior of unreinforced irregular masonry. Eng Struct 2020;223:111181. https://doi.org/10.1016/j.engstruct.2020.111181.
[65] Rizvi ZH, Sattari AS, Wuttke F. Meso scale modelling of infill foam concrete wall for earthquake loads. In 16th European Conference on Earthquake Engineering (16ECEE), Thessaloniki, Greece, 2018.
[66] Binici B, Canbay E, Aldemir A, Demirel IO, Uzgan U, Eryurtlu Z, et al. Seismic behavior and improvement of autoclaved aerated concrete infill walls. Eng Struct 2019;193:68–81.

[67] Penna A, Calvi GM, (2006), Campagna sperimentale su telai in c.a. con tamponamenti in Gasbeton (AAC) con diverse soluzioni di rinforzo. Experimental Report University of Pavia Italy 2006.
[68] Dolatshahi KM, Aref AJ. Two-dimensional computational framework of meso-scale rigid and line interface elements for masonry structures. Eng Struct 2011;33(12):3657–67.
[69] Khojasteh, A. Nonlinear modelling of masonry infill walls in building structures subject to extreme loading. PhD dissertation, Imperial College London, London, UK, 2017.
[70] Cornelissen H, Hordijk D, Reinhardt H. Experimental determination of crack softening characteristics of normalweight and lightweight. Heron 1986;31(2):45–6.
[71] ASTM Standard C192/C192M. Making and curing concrete test specimens in the laboratory. ASTM International, West Conshohocken, PA, USA, 2002.
[72] ASTM Standard C617/C617M. Standard Practice for Capping Cylindrical Concrete Specimens. ASTM International, West Conshohocken, PA, 2012.
[73] Turkish Earthquake Code (TEC), Regulations on Structures constructed in Disaster Regions, Prime Ministry Disaster and Emergency Management Authority Ankara Turkey 2018.
[74] Mojsilovic N, Salmanpour AH. Masonry walls subjected to in-plane cyclic loading: application of digital image correlation for deformation field measurement. International Journal of Masonry Research and Innovation 2016;1(2):165–87.
[75] Ramos Tiago, Furtado André, Eslami Shayan, Alves Sofia, Rodrigues Hugo, Arêde António, et al. 2D and 3D digital image correlation in civil engineering–measurements in a masonry wall. Procedia Eng 2015;114:215–22.
[76] Korswagen Paul A, Longo Michele, Meulman Edwin, Rots Jan G. Crack initiation and propagation in unreinforced masonry specimens subjected to repeated in-plane loading during light damage. Bull Earthq Eng 2019;17(8):4651–87.
[77] Furtado André, Ramos T, Rodrigues Hugo, Arêde António, Varum Humberto, Tavares P. In-plane response of masonry infill walls: experimental study using digital image correlation. Procedia Eng 2015;114:870–6.
[78] Kumar Srinidhi Lakshmish, Aravind HB, Hossiney Nabil. Digital image correlation (DIC) for measuring strain in brick masonry specimen using Ncorr open source 2D MATLAB program. Results in Engineering 2019;4:100061. https://doi.org/10.1016/j.rineng.2019.100061.
[79] Turkish Standardization Institute. Methods of test for masonry – Part 1: Determination of compressive strength, TS EN 1052-1. Ankara: Turkish Standards Institution; 2000.
[80] Todorovic L. Out of plane seismic performance of aac infill walls with openings. MSc dissertation. Ankara, Turkey: Middle East Technical University; 2019.
[81] Calvi GM, Bolognini D, (2001), Seismic response of R.C. frames infilled with weakly reinforced hollow masonry panels. Journal of Earthquake Engineering 2001;5(2):153–185.
[82] Costa AA. Experimental testing of lateral capacity of masonry piers. An application to seismic assessment of aac masonry buildings. MSc Dissertation, ROSE School, IUSS Pavia, Italy, 2007.
[83] Demirel IO, Canbay E, Binici B, Yakut A, Eryurtlu Z. Gazbeton dolgulu betonarme çerçevelerin deprem performansı üzerine deneysel çalışma. In: 3. Türkiye Deprem Mühendisliği ve Sismoloji Konferansı (3. TDMSK), İzmir, Turkey, 2015.
[84] ASTM E519-10, Standard test method for diagonal tension (shear) in masonry assemblages, 2010.
[85] Morandi Paolo, Hak Sanja, Magenes Guido. Performance-based interpretation of in-plane cyclic tests on RC frames with strong masonry infills. Eng Struct 2018;156:503–21.
[86] Federal Emergency Management Agency. FEMA 306: evaluation of earthquake damaged concrete and masonry wall buildings-basic procedures manual. Washington DC: Applied Technology Council (ATC-43 project); 1998.
[87] Paulay T, Priestley MJN. Seismic design of reinforced concrete and masonry buildings. New York (NY): John Wiley & Sons; 1992. p. 744p.
[88] Turkish Standardization Institute. Requirements for design and construction of reinforced concrete structures TS 500. Ankara: Turkish Standardization Institute; 2000.
[89] American Concrete Institute ACI Committee. Building code requirements for structural concrete ACI 318-11and commentary 318R-11. ACI 318-08/318R11. Farmington Hills (MI, USA): American Concrete Institute; 2011.
[90] CEB-FIP Model Code 2010-fib, vol. 1; 2012, p. 120.